Catalysis Today 148 (2009) 243–250

Contents lists available at ScienceDirect

Catalysis Today

journal homepage: www.elsevier.com/locate/cattod

Carbon dioxide reforming of methane over nickel-grafted SBA-15 and MCM-41 catalysts

Dapeng Liu [a], Xian-Yang Quek [a], Hui Hui Adeline Wah [a], Guangming Zeng [b], Yongdan Li [b], Yanhui Yang [a,*]

[a] School of Chemical and Biomedical Engineering, Nanyang Technological University, Singapore 637459, Singapore
[b] Tianjin Key Laboratory of Applied Catalysis Science and Technology, School of Chemical Engineering, Tianjin University, Tianjin 300072, China

ARTICLE INFO

Article history:
Available online 19 September 2009

Keywords:
Nickel catalyst
Grafting
Methane reforming
Carbon dioxide
SBA-15
MCM-41

ABSTRACT

Mesoporous molecular sieves SBA-15 and MCM-41 supported Ni catalysts were prepared via a post-synthesis grafting method. The catalytic properties of these catalysts were investigated in CO_2 reforming of CH_4 under atmospheric pressure and compared with the impregnated catalysts. Characterization using powder X-ray diffraction, N_2 physisorption, H_2 temperature-programmed reduction, TG/DTA, Raman spectra and transmission electron microscopy techniques revealed that both catalyst preparation method and the nature of support play important roles in controlling the catalytic performance. The highest catalytic activity and long-term stability were obtained over a 5 wt.% Ni-grafted SBA-15 catalyst. This superior catalytic behavior was closely related with the strong resistance toward carbon formation and active metal sintering. Furthermore, the improved properties of the catalyst was caused by the formation of highly dispersed small Ni particles anchored by silica matrix, rather ordered pore structure, and structural stability of SBA-15 material under reaction conditions.

1. Introduction

Catalytic reforming of methane with carbon dioxide, also known as dry reforming, has recently attracted considerable attention due to the simultaneous utilization and reduction of two greenhouse gases. The synthesis gas (syngas) produced contains a lower H_2/CO ratio than those available from steam reforming and partial oxidation of methane, which is preferred for the synthesis of valuable oxygenated chemicals and long-chain hydrocarbons [1,2].

Although most group VIII metals show appreciable activity for CH_4–CO_2 reforming, non-noble metal, Ni, is of particular interest from the industrial point of view, due to its low cost, inherent availability, as well as its catalytic performance comparable to those of noble metals [3,4]. Strategies utilized to develop Ni catalysts with good resistance to carbon formation include: (1) altering the acid–base or redox properties of carrier [5–8], (2) introducing the second active metal (e.g. Ru [9], Rh [10] and Pt [11]), and (3) controlling Ni particle size/distribution via other preparation routes, such as sol–gel method [12,13] or with plasma treatment [14].

Recently we have investigated the feasibility of catalyzing dry reforming with nickel containing mesoporous molecular sieve catalysts [15]. Remarkable catalytic activity was observed over Ni-incorporated MCM-41 catalysts at temperatures as low as 500 °C. Moreover, both stable and high catalytic activity were observed over hydrothermally synthesized Ni-MCM-41 in contrast to the impregnated catalyst. The improved catalytic performance was suggested to closely associate with the amount of active centers on the pore wall surface and the stabilized-dispersion of these active sites by the silica matrix and/or the surrounding unreduced nickel ions, thus facilitating the formation of the active Ni nano-clusters with high dispersion under reaction conditions and promoting the reforming reaction while suppressing the carbon formation.

Furthermore, Zr-promoted Ni-MCM-41 catalysts exhibited an enhanced initial activity compared to Ni-MCM-41. Adding Zr^{4+} remarkably improved the long-term stability whereas the decreased initial activity and long-term stability were observed for Ti- and Mn- substituted catalysts. It was observed that Zr^{4+} enhanced the structure stability and the dispersion of active Ni sites. The strong anchoring effect of Zr^{4+} and partial activation of CO_2 by Zr^{4+} contributed to the high initial activity and long-term stability. However, the decoration of Ni clusters with TiO_x and MnO_x species in Ni-Ti- and Ni-Mn-MCM-41 catalysts hindered the accessibility of Ni active centers, thus decreasing their catalytic performance. The crystalline transformation of silica also played a negative role in Ni-Mn- and Ni-Ti-MCM-41 catalysts [16].

Both MCM-41 and SBA-15 are ordered mesoporous molecular sieves with the uniform two-dimensional hexagonal pore arrangements, narrow pore size distribution and large surface area [17,18]. The abundant surface silanol groups and mesostructured properties provide a unique platform for immobilizing transition metal

* Corresponding author. Tel.: +65 6316 8940; fax: +65 6794 7553.
E-mail address: yhyang@ntu.edu.sg (Y. Yang).

0920-5861/$ – see front matter © 2009 Elsevier B.V. All rights reserved.
doi:10.1016/j.cattod.2009.08.014

precursors inside the pores of these materials. However, some differences are present, e.g., MCM-41 has the pore diameter of 2–6 nm and relatively smooth pore wall surfaces while SBA-15 possesses larger pore size, typically in the range of 5–10 nm and exhibits considerable surface roughness due to the presence of microporous interconnections [19].

In this contribution, a method of grafting nickel oxide species onto the surfaces of mesopores MCM-41 and SBA-15 catalysts was reported with acetylacetone salt under anhydrous conditions. Their catalytic behaviors for methane reforming with carbon dioxide were investigated and also compared with those of the conventional impregnated catalysts.

2. Experimental

2.1. Catalyst preparation

MCM-41 and SBA-15 were prepared according to the previously reported methods [20,21]. Tetraethyl orthosilicate (TEOS) was used as silica sources for both support materials. Cethyltrimethylammonium bromide (CTAB) and poly(ethylene glycol)-block-poly(propylene glycol)-block-poly(ethylene glycol) triblock copolymer P123 were used as the structure-directing agents for MCM-41 and SBA-15, respectively. The support materials were collected after calcining at 540 °C for 6 h in flowing air. Ni-grafted MCM-41 and SBA-15 catalysts were synthesized with nickel acetylacetonate as metal precursor, following a controlled grafting process through atomic layer deposition (ALD) [22]. The suspension of calcined MCM-41 or SBA-15 sample in anhydrous toluene was refluxed at 110 °C under flowing nitrogen for 5 h before grafting. Subsequently, the appropriate amount of the nickel precursor solution was added dropwise to the above suspension. The reaction mixture was allowed to reflux overnight in nitrogen atmosphere. After cooling, filtering and washing, the powder was recovered and dried at room temperature overnight followed by calcining at 540 °C for 4 h to obtain the final nickel-grafted catalysts. For comparison, the Ni-impregnated catalysts with the same nickel loading were prepared by a conventional wet impregnation method, as previously described [15]. Hereafter, the Ni-grafted catalysts are designated as *x*Ni-SBA-15 or *x*Ni-MCM-41 whereas the impregnated ones *x*Ni/SBA-15 or *x*Ni/MCM-41 with *x* denoting the weight percentage of Ni loading.

2.2. Catalyst characterization

Powder X-ray diffraction (XRD) data were collected with a Bruker AXS D8Focus system equipped with a CuK_α source (λ = 1.5406 Å) operated at 40 kV and 40 mA. Nitrogen physisorption measurements were carried out using a Quantachrome AUTOSORB-6B static volumetric instrument. Hydrogen temperature-programmed reduction (TPR) experiments were conducted on a Quantachrome Autosorb-1C system equipped with a thermal conductivity detector. Approximately 200 mg of the sample was used, with a heating rate of 8 °C min^{-1} and the temperature range from 100 to 900 °C. The gas mixture employed in TPR was 5 vol.% H_2/Ar with a flow rate of 30 mL/min. The amount of carbon deposited on the catalysts was determined on a PerkinElmer TG/DTA instrument under air atmosphere. Raman spectra of the spent catalysts were recorded using an excitation wavelength of 633 nm on a Renishaw spectrometer. Transmission electron microscopy (TEM) images were taken on a JEOL JEM-1400 operated at 120 kV. The sample was dispersed in ethanol by sonication, and 0.05 mL of this suspension was dropped on a copper mesh coated with an amorphous holey carbon film. Particle size distributions were estimated by counting more than 200 particles at random.

2.3. Catalytic reaction

Catalytic activity measurements were carried out in a fixed bed quartz reactor under atmosphere pressure. Prior to the reaction, the catalysts were reduced in-situ at 750 °C for 2 h under hydrogen flow. The molar ratio of the feed gas mixture CH_4/CO_2/He and the space velocity (GHSV) was fixed at 1:1:2 and 50000 h^{-1}, respectively. The initial activity was tested in the temperature range of 500–800 °C in steps of 100 °C. The catalytic stability was evaluated at 750 °C for 72 h. The products were analyzed using an on-line Agilent 6890 gas chromatography with a thermal conductivity detector.

3. Results and discussion

The XRD patterns of parent SBA-15, MCM-41 and Ni supported SBA-15 and MCM-41 samples are shown in Fig. 1(A). For SBA-15 samples, three peaks can be discerned with the strongest one corresponding to (1 0 0) diffraction followed by two well-resolved (1 1 0) and (2 0 0) peaks, which can be indexed to a hexagonal lattice. Similar diffraction peaks are also observable on MCM-41 samples, demonstrating that the structural integrity has been retained after the incorporation of Ni and calcination process, even with 5 wt.% Ni loading. Although Ni-modified samples exhibit similar diffractions to the corresponding parent material, these Ni-containing catalysts show relatively weak and broad diffraction peaks, implying a decrease of framework order. The diffraction peaks of NiO particles are absent over all Ni-grafted samples but observed over Ni-impregnated samples (not shown), indicating that the highly dispersed Ni species can be prepared efficiently by this grafting method.

As shown in Fig. 1(B), all mesoporous material supported catalysts except for 5Ni-MCM-41 sample, exhibit a sharp step increase in nitrogen uptake at medium relative pressures, arising from the capillary condensation of nitrogen inside the primary mesopores, representative of type IV isotherm [23]. Three distinct regions can be discerned in the isotherms for these mesoporous materials: (1) monolayer–multilayer adsorption of nitrogen on the pore walls at low pressures, (2) a sudden steep increase of the adsorbed nitrogen at intermediate pressures due to the capillary condensation, and (3) multilayer adsorption on the external surface of the particles. The existence of capillary condensation at higher relative pressures in SBA-15 samples relative to MCM-41 samples suggests the larger pore diameter of SBA-15 samples. The broad hysteresis loop of SBA-15 sample is caused by the presence of long mesopores connected by smaller micropores, thus hampering the filling and emptying of the accessible volume [19,24,25]. In case of the 5Ni-MCM-41 sample, a pronounced inclination of the condensation step can be attributed to a certain heterogeneity of pore size distribution, which is also evidenced by the broad (1 0 0) diffraction peak in the corresponding XRD pattern.

The textural characteristics of various mesoporous catalysts are summarized in Table 1. After introducing Ni, an obvious decrease in the BET surface area and pore volume is observed, regardless of the content of Ni loading. As long as the pore diameter is concerned, the grafted SBA-15 samples have a similar pore size to that of parent SBA-15 with Ni loading no more than 3 wt.%. Further increasing Ni content to 5 wt.% over SBA-15 results in a decrease of pore size, regardless of preparation method of SBA-15 supported Ni catalysts. For MCM-41 series, the pore size of all supported samples decreases to some extent, more significantly for 5Ni-MCM-41, which is most likely due to the vulnerable structural stability of MCM-41 under reflux and non-aqueous conditions. The significant reduction in specific surface area, pore volume with increasing Ni loading implys that the local blockage of pore

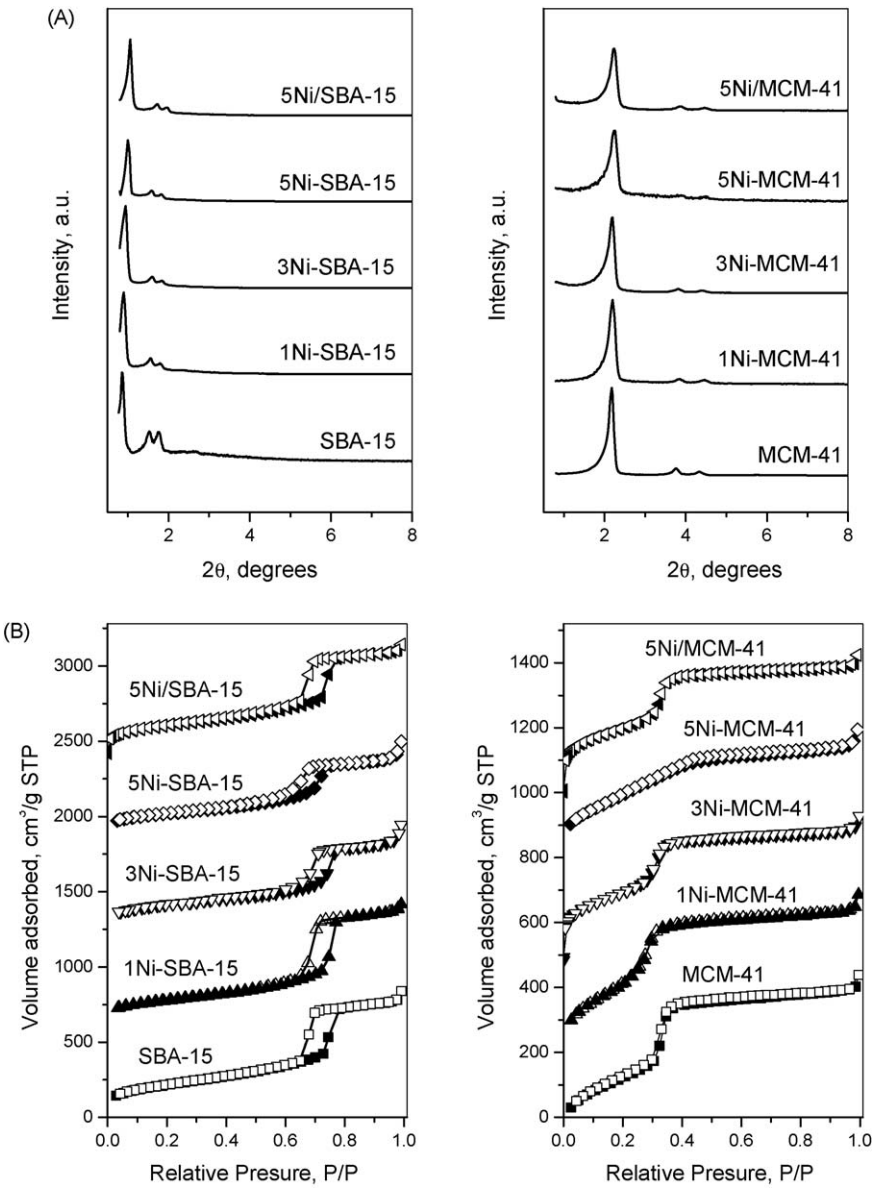

Fig. 1. XRD patterns (A) and N_2 sorption isotherms (B) of different samples.

channel induced by grafting or depositing Ni species at the pore entrance and/or partial structural degradation easily take place under higher Ni loading.

TPR is an effective technique for characterizing the reducibility of supported metal oxide catalysts. TPR profiles of the mesoporous material supported catalysts are shown in Fig. 2. All the grafted samples exhibit similar profile of hydrogen reduction showing only one pronounced reduction peak irrespective of the Ni loading. For all the grafted catalysts, the reduction peak shifts gradually towards high temperature with Ni loading, in the range of 550–640 °C, which may be related to the facile formation of nickel hydrosilicate in the case of higher Ni content [26]. Moreover, compared to SBA-15 grafted samples; one can observe a slightly higher reduction temperature over MCM-41 grafted samples

Table 1
Textural properties of different samples.

Sample	Nickel content (wt. %)	Surface area (m^2/g)	Pore volume (mL/g)	Pore diameter (nm)
SBA-15	0	754	1.31	6.82
1Ni-SBA-15	1.0	604	1.28	6.84
3Ni-SBA-15	3.0	535	0.96	6.76
5Ni-SBA-15	5.0	536	0.98	6.32
5Ni/SBA-15	5.0	692	1.10	6.28
MCM-41	0	982	0.96	2.82
1Ni-MCM-41	1.0	873	0.81	2.54
3Ni-MCM-41	3.0	795	0.74	2.64
5Ni-MCM-41	5.0	766	0.67	2.33
5Ni/MCM-41	5.0	710	0.73	2.65

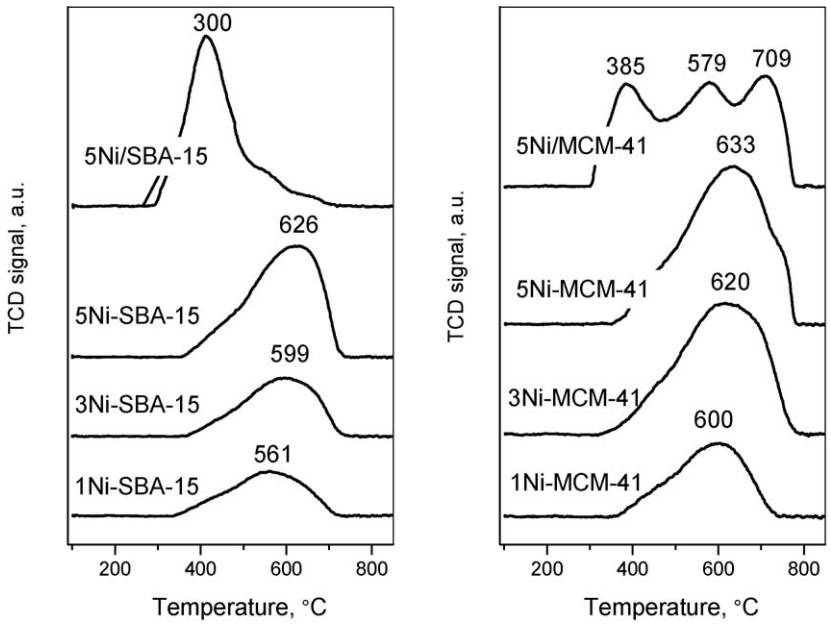

Fig. 2. TPR profiles of various Ni supported catalysts.

under the same Ni content. A reasonable explanation is that the arrangement of Si–OH on inner surface is relatively regular for MCM-41 while the pore surface of SBA-15 is rough with a substantial amount of $Si(OH)_2$ groups associated with surface defects [27]. Regardless of metal loading and carrier type, all Ni-grafted catalysts possess higher reduction temperature than the impregnated samples, indicating the formation of strong interaction between metal and support after the Ni species was grafted onto the surface. The low temperature reduction at 300 °C for 5Ni/SBA-15 implies the presence of NiO particles and the interaction between metal and support is rather weak. The impregnated MCM-41 sample exhibits different reduction pattern from grafted MCM-41 samples with three peaks at around 385, 579 and 709 °C. The first peak corresponds to the reduction of NiO particles and two others are attributed to the reduction of Ni species strongly interacting with the carrier.

The dependence of initial catalytic activity on the reaction temperature is depicted in Fig. 3(A). The conversion of CH_4 increases with increasing the reaction temperature, reflecting the endothermic character of dry reforming. All the catalysts show their highest catalytic activity at 800 °C in the temperature range studied. In particular, all grafted catalysts exhibit CH_4 conversion above 90% at this temperature. In most cases, 5Ni-SBA-15 possesses the highest catalytic activity and 1Ni-MCM-41 shows the lowest activity among the grafted samples. Interestingly, the activities of 5Ni/MCM-41 and 5Ni-MCM-41 are similar despite a subtle higher activity for the latter catalyst. However, the conversion of CH_4 over 5Ni/SBA-15 is close to that of 1Ni-MCM-41 but lower than over 1Ni-SBA-15. It can be assumed that the lower catalytic activity of 5Ni/SBA-15 is due to the inferior dispersion of Ni species arose by weak metal-support interaction (Fig. 2). While the excellent catalytic activity of 5Ni-SBA-15 is closely associated with the improved dispersion of Ni active sites under grafting conditions, which is consistent with strong interaction between metal and support (Fig. 2) as well as good retention of mesoporous structural order (Fig. 1 and Table 1). To compromise the catalytic activity and energy consumption, 750 °C was selected as the favorable reaction temperature to evaluate the long-term stability of the catalysts in this investigation.

The long-term stabilities of supported catalysts are shown in Fig. 3(B). All the catalysts exhibit the initial conversion of above 75%. Superior catalytic activity can be found over 5Ni-SBA-15 followed by 5Ni/MCM-41, 5Ni/SBA-15. 5Ni-MCM-41 sample has a significant activity loss with the deactivation rate of about 0.28% h^{-1}. After 72 h time on stream (TOS), the activity sequence is as following: 5Ni-SBA-15 (78%) > 5Ni/MCM-41 (71%) > 5Ni/SBA-15 (65%) > 5Ni-MCM-41 (54%). The H_2/CO ratios for all the catalysts are lower than unity, which is mainly caused by reverse water–gas shift reaction (RWGS) [28]. The low H_2/CO ratios over 5Ni-MCM-41 and 5Ni/SBA-15 suggest that the RWGS easily occurs on these two catalysts, which results from the presence of more unreacted CO_2 under low catalytic activity. The similar observation was also found in other reports [29,30].

Carbon deposition over the spent catalysts after 72 h TOS was quantified by TG–DTA analysis. As shown in Fig. 4, the weight loss of spent catalysts increases with the following sequence: 5Ni-SBA-15 (9.0%) < 5Ni/SBA-15 (14.3%) < 5Ni-MCM-41 (23.0%) < 5Ni/MCM-41 (34.6%). It is evident that the grafted catalysts have lower amount of carbon deposition compared to the corresponding impregnated samples. Especially, the grafted 5Ni-SBA-15, with the excellent activity and stability during long-term test, has the lowest carbon formation. From DTA profiles, one can observe a small exothermic peak around 338 °C before the main peak after 600 °C over SBA-15 supported catalysts, while this weak peak is absent for MCM-41 supported samples. Based on previous reports [5,15,31], this low temperature peak can be attributed to the oxidation of active carbon, or amorphous carbon, whereas the inert carbon, namely, graphitic carbon will be oxidized at high temperatures. More amorphous carbon species have been formed over the SBA-15 supported samples, and the presence of the relative active carbon species is beneficial to prevent the deactivation of catalyst to some extent.

The crystalline phases of spent catalysts after 72 h TOS stability test were determined by XRD characterization. As shown in Fig. 5(A), both the diffraction peaks of graphitic carbon and Ni particles can be seen over all the spent catalysts. The graphite peak is more pronounced over the MCM-41 supported catalysts, especially with the impregnated sample, which confirms the graphitic nature of carbonaceous species over these catalysts as suggested by DTA results. The average sizes of Ni particles calculated with the Scherrer equation have the following sequence: 5Ni-MCM-41 (7.3 nm) < 5Ni-SBA-15 (8.4 nm) < 5Ni/

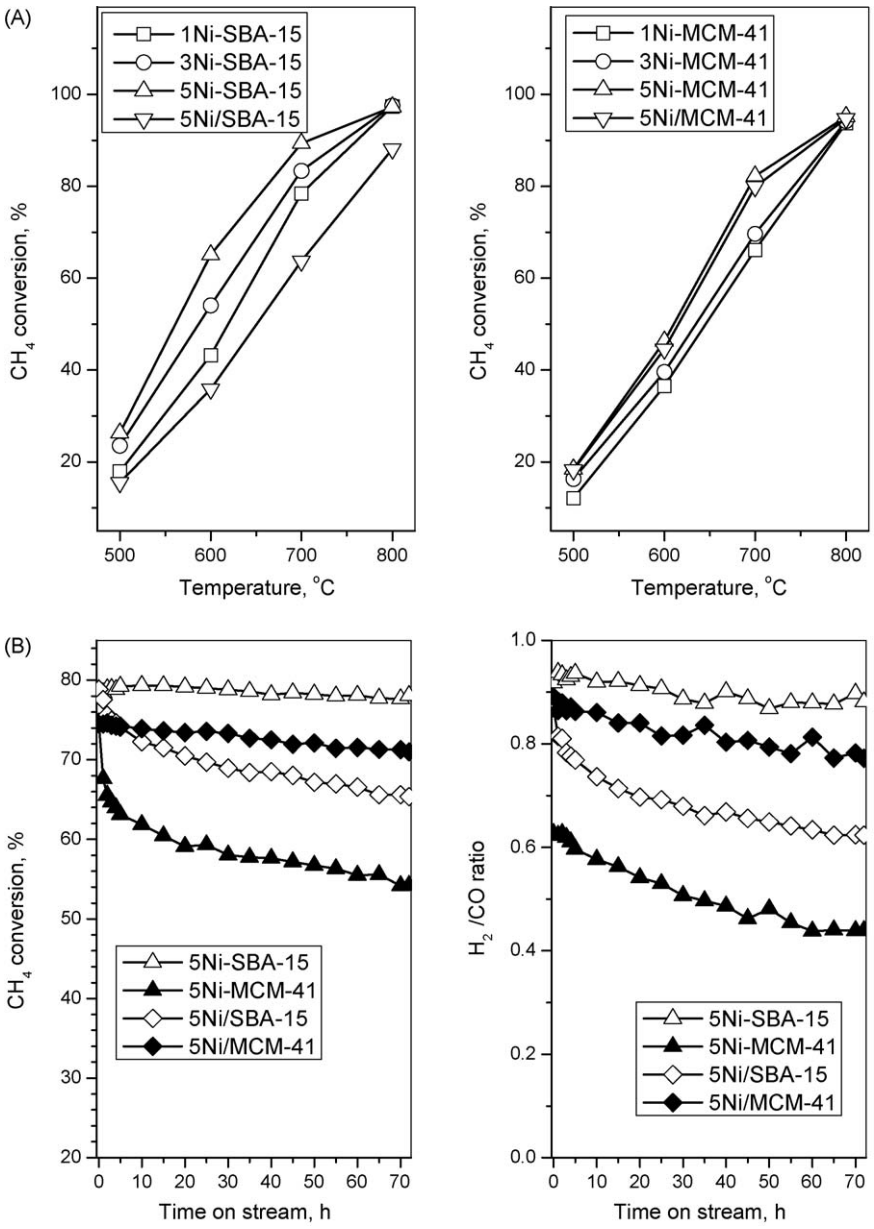

Fig. 3. (A) Effect of temperature on CH_4 conversion over various Ni catalysts; (B) The results of stability test over representative catalysts.

MCM-41 (14.0 nm) < 5Ni/SBA-15 (19.4 nm). The appearance of large nickel particle size, especially for the impregnated catalysts, suggests that remarkable sintering of Ni particles occurred during the stability test.

Raman spectra of the spent catalysts are presented in Fig. 5(B). All the samples show similar profiles with a strong D band (1328 cm^{-1}) and a weak G band (1574 cm^{-1}). The simultaneous presence of these two Raman bands reveals that both the amorphous carbon and graphite have been formed during the reaction [15]. The relatively higher intensity of G band over the impregnated catalysts rather than on the grafted samples suggests the carbon species of graphite character can be easily formed over the impregnated catalysts.

TEM images of the spent catalysts after stability test are depicted in Fig. 6(A). The corresponding particle size distributions obtained from TEM are summarized in Fig. 6(B) (including the calculated average particle size and the standard deviation). The smaller and relatively uniform nickel particle size can be observed for the grafted samples with 5Ni-MCM-41 which possesses the smallest average particle size of 7.6 nm among all the spent catalysts. For the impregnated 5Ni/MCM-41, the average Ni particle size is 12.1 nm. The impregnated 5Ni/SBA-15 presents the largest nickel particle diameter of 31.2 nm and much wider size distribution due to the large pore diameter and heterogeneity of pore diameters. Filamentous carbon structures can be easily found in TEM images of MCM-41 supported catalysts, which is in line with the large amount of carbon deposition over these catalysts.

Combining the above characterization results with activity tests, the influencing factors leading to the activity loss can be deduced. Although carbon deposition and active metal sintering are two main factors affecting the catalytic activity of Ni-based catalysts, they play different roles for these mesoporous materials supported Ni catalysts. In case of Ni/SBA-15, the deactivation mainly arises from the nickel metal sintering because only moderate amount of carbon deposition can be observed; particularly the larger portion of carbon deposition is relatively active carbon species over the spent Ni/SBA-15 catalyst. For Ni-MCM-41 catalyst, the origin of catalyst deactivation is mainly

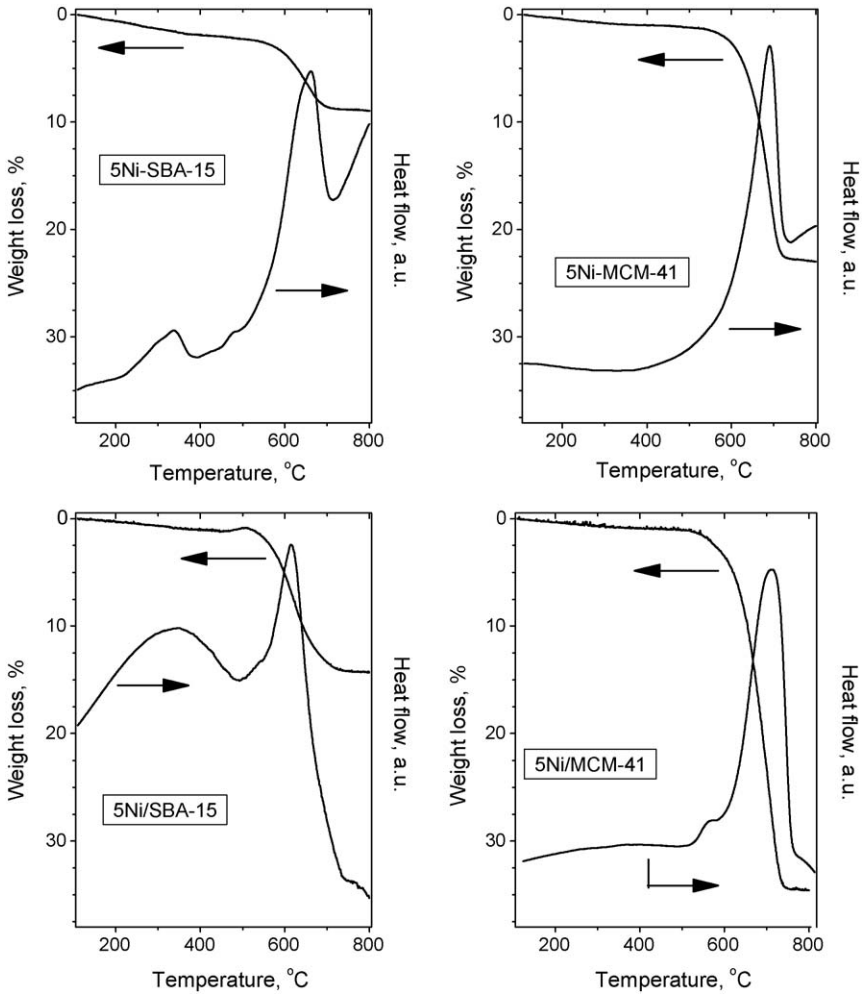

Fig. 4. TG/DTA profiles of spent catalysts after 72 h reaction.

attributed to the large quantity of carbon formation in view of the small Ni particle size and the narrow particle size distribution observed on the spent catalyst. It should be mentioned that a fraction of Ni species might be buried inside the silica matrix accompanied by local structural degradation of 5Ni-MCM-41, thus decreasing total amount of Ni active sites. For the 5Ni/MCM-41, both carbon deposition and metal sintering are responsible for activity loss considering the simultaneous occurrence of the high carbon content and large nickel particle sizes. However, the maintenance of considerable catalytic activity and stability over 5Ni/MCM-41 suggests that most of active centers are dispersed and easily accessible to reactant molecules. Besides, some exposed Ni species sticking to carbon deposition should also be catalytically active in the reforming. In contrast to the above Ni-based catalysts which show continuous activity decay with TOS, no significant deactivation was observed over 5Ni-SBA-15. Its excellent activity

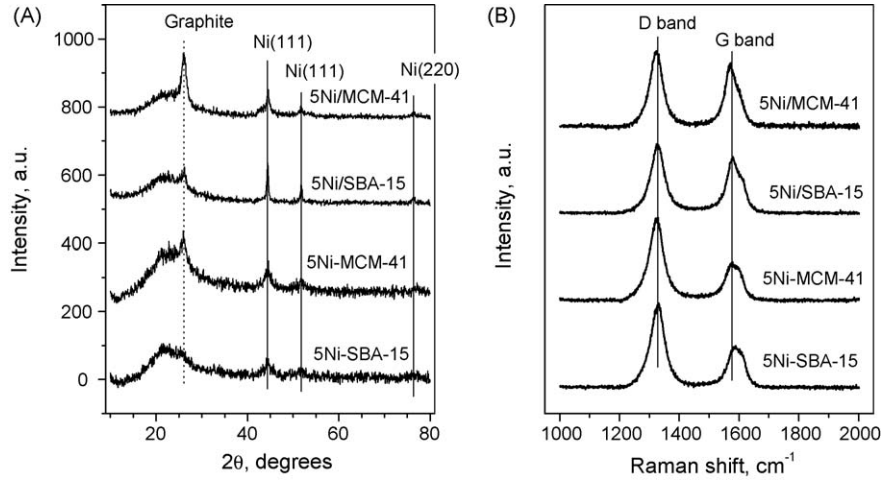

Fig. 5. (A) XRD patterns of spent catalysts; (B) Raman spectra of carbon deposited on spent catalysts.

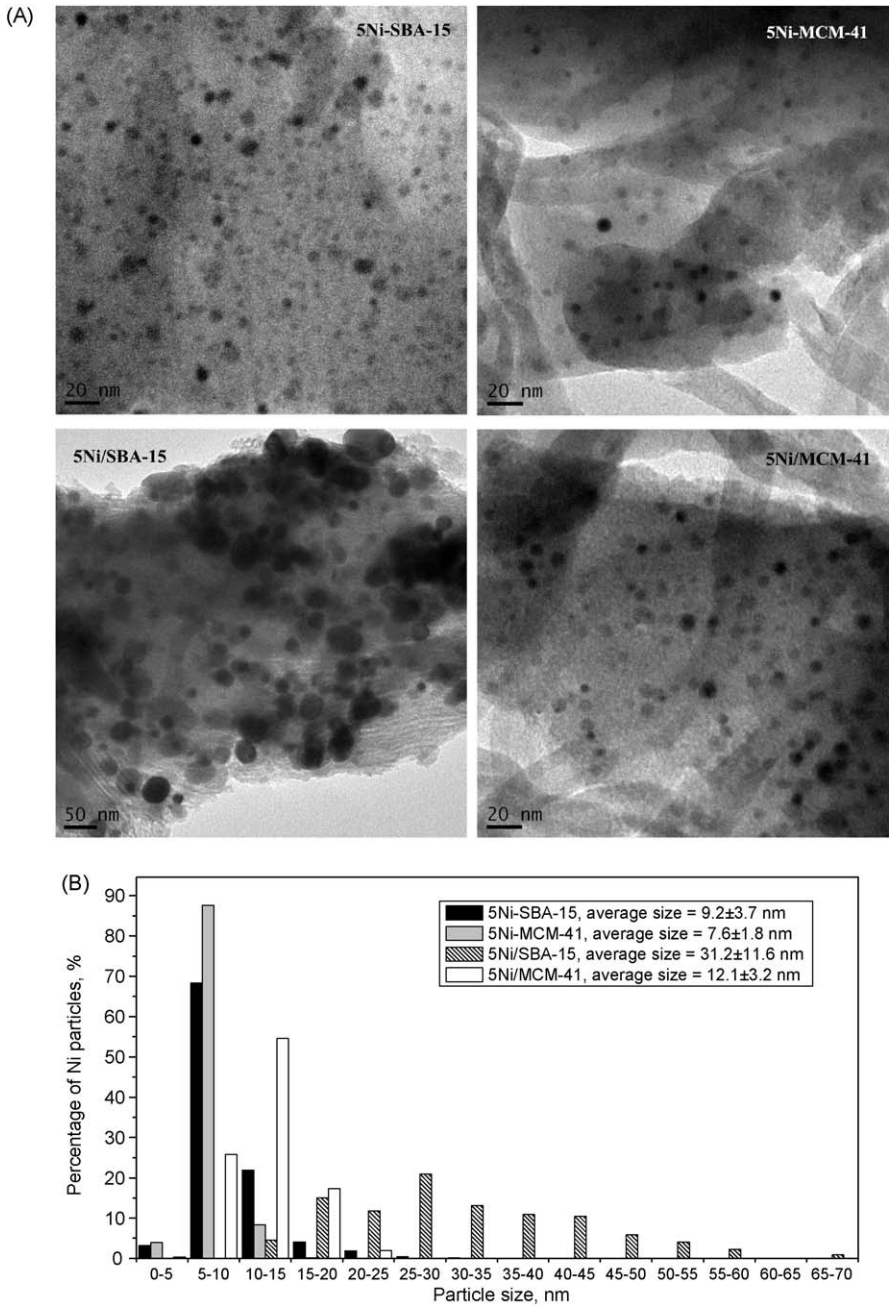

Fig. 6. (A) TEM images of the spent catalysts. (B) Particle size histograms of the spent catalysts.

and high stability can be attributed to strong inhibition effect of the Ni-grafted SBA-15 catalyst on carbon formation and metal sintering. The suppression of carbon formation can be stemmed from the presence of highly stabilized-dispersion of active sites on the silica matrix (Figs. 4 and 6), stable silica framework structural properties of SBA-15 material. In summary, the advantages of good structural stability and unique pore structural properties of SBA-15 over MCM-41 with moderate stability and isolated pore structure make the former a promising catalytic material for CH_4 reforming with CO_2.

4. Conclusion

Two different mesoporous molecular sieves SBA-15 and MCM-41 are selected as carriers to prepare the supported Ni catalysts for CO_2 reforming of CH_4. The catalytic conversion of CH_4 depends on the catalyst preparation method employed and the nature of support. Nickel catalysts with substantially smaller nickel cluster size can be synthesized by the grafting method in comparison with the conventional impregnation. Among all the supported catalysts, the grafted 5Ni-SBA-15 exhibits the excellent catalytic performance in catalytic conversion and long-term stability, originating from the strong inhibition on carbon formation and active metal sintering. The high structural stability, much uniform mesopore distribution and unique pore structure endow SBA-15 material with distinct advantages over the MCM-41 as the grafting material for CH_4 dry reforming with CO_2. It should be mentioned that, despite the interesting features of SBA-15 material, the grafted Ni content is restricted by the concentration of surface silanol groups of SBA-15, In the current grafting process, we assume one Ni atom requires two silanol groups to complete the grafting step, the surface density of Ni species should be $2NiO_x/nm^2$ based on the

estimated 4.0Si–OH/nm^2 silanol groups on SBA-15 [27], the ideally maximum content of Ni is about 12.8 wt.% for the current SBA-15 parent material. However the actual grafting amount of Ni may be subsententially lower than this upper bound. Therefore, much work still remains to be done to explore suitable methods in preparing the supported Ni catalyst with high Ni content and good dispersion to obtain high productivity and stability. Tomiyama and co-workers [32] prepared Ni/SiO_2 catalysts with Ni loading of 5–50 wt.% by a homogeneous precipitation method, the steady catalytic activity can be recognized for Ni/SiO_2 samples with Ni loading of $\leq$20 wt.%. More recently, a novel plasma preparation method was developed for preparing Ni/Al_2O_3 catalysts with Ni content of 9 wt.% which exhibited enhanced activity and stability compared to the catalyst without plasma treatment [33]. These preparation methods may provide new direction for the catalyst development.

Acknowledgements

The authors thank AcRF tier 2 (M45120006 ARC 13/07) for providing funding support. The financial support of AcRF tier 1 (RG45/06) is gratefully acknowledged.

References

[1] J.R.H. Ross, A.N.J. van Keulen, M.E.S. Hegarty, K. Seshan, Catal. Today 30 (1996) 193.
[2] I. Wender, Fuel Process. Technol. 48 (1996) 189.
[3] Y.H. Hu, E. Ruckenstein, Adv. Catal. 48 (2004) 297.
[4] M.C.J. Bradford, M.A. Vannice, Catal. Rev. Sci. Eng. 41 (1999) 1.
[5] Z.L. Zhang, X.E. Verykios, Catal. Today 21 (1994) 589.
[6] J.A. Lercher, J.H. Bitter, W. Hally, W. Niessen, K. Seshan, Stud. Surf. Sci. Catal. 101 (1996) 463.
[7] S.B. Wang, G.Q.M. Lu, Appl. Catal. B 19 (1998) 267.
[8] M.C.J. Bradford, M.A. Vannice, Catal. Today 50 (1999) 87.
[9] C. Crisafulli, S. Scirè, S. Minicò, L. Solarino, Appl. Catal. A 225 (2002) 1.
[10] S. Irusta, L.M. Cornaglia, E.A. Lombardo, J. Catal. 210 (2002) 263.
[11] A.N. Pinheiro, A. Valentini, J.M. Sasaki, A.C. Oliveira, Stud. Surf. Sci. Catal. 174 (2008) 205.
[12] J.-H. Kim, D.J. Suh, T.-J. Park, K.-L. Kim, Appl. Catal. A 197 (2000) 191.
[13] B.S. Liu, C.T. Au, Catal. Lett. 85 (2003) 165.
[14] X.L. Zhu, P.P. Huo, Y.P. Zhang, D.G. Cheng, C.J. Liu, Appl. Catal. B 81 (2008) 132.
[15] D.P. Liu, R. Lau, A. Borgna, Y.H. Yang, Appl. Catal. A 358 (2009) 110.
[16] D.P. Liu, X.Y. Quek, W.N.E. Cheo, R. Lau, A. Borgna, Y.H. Yang, J. Catal. 266 (2009) 380.
[17] C.T. Kresge, M.E. Leonowicz, W.J. Roth, J.C. Vartuli, J.S. Beck, Nature 359 (1992) 710.
[18] D.Y. Zhao, J.L. Feng, Q.S. Huo, Science 279 (1998) 548.
[19] M. Impéror-Clerc, P. Davidson, A. Davidson, J. Am. Chem. Soc. 122 (2000) 11925.
[20] S.Q. Hu, D.P. Liu, L.S. Li, A. Borgna, Y.H. Yang, Catal. Lett. 129 (2009) 478.
[21] D.Y. Zhao, J.L. Feng, Q.S. Huo, N. Melosh, G.H. Fredickson, B.F. Chmelka, G.D. Stucky, J. Am. Chem. Soc. 120 (1998) 6024.
[22] J.E. Herrera, J.H. Kwak, J.Z. Hu, Y. Wang, C.H.F. Peden, J. Macht, E. Iglesia, J. Catal. 239 (2006) 200.
[23] J.B. Condon, Surface Area And Porosity Determinations By Physisorption: Measurements And Theory, Elsevier, Amsterdam, 2006.
[24] A. Vinu, D.P. Sawant, K. Ariga, K.Z. Hossain, S.B. Halligudi, M. Hartmann, M. Nomura, Chem. Mater. 17 (2005) 4049.
[25] A. Galarneau, H. Cambon, F. Di Renzo, F. Fajula, Langmuir 17 (2001) 8328.
[26] J. van de Loosdrecht, A.M. van der Kraan, A.J. van Dillen, J.W. Geus, J. Catal. 170 (1997) 217.
[27] I.G. Shenderovich, G. Buntkowsky, A. Schreiber, E. Gedat, S. Sharif, J. Albrecht, N.S. Golubev, G.H. Findenegg, H.-H. Limbach, J. Phys. Chem. B 107 (2003) 11924.
[28] J.M. Wei, B.Q. Xu, J.L. Li, Z.X. Cheng, Q.M. Zhu, Appl. Catal. A 196 (2000) L167.
[29] X. Chen, K. Honda, Z.G. Zhang, Appl. Catal. A 288 (2005) 86.
[30] A.A. Lemonidou, I.A. Vasalos, Appl. Catal. A 228 (2002) 227.
[31] W.D. Zhang, B.S. Liu, C. Zhu, Y.L. Tian, Appl. Catal. A 292 (2005) 138.
[32] R. Takajashi, S. Sato, T. Sodesawa, S. Tomiyama, Appl. Catal. A 286 (2005) 142.
[33] D.G. Cheng, X.L. Zhu, Y.H. Ben, F. He, L. Cui, C.J. Liu, Catal. Today 30 (2006) 205.